IEEE Access
Multidisciplinary | Rapid Review | Open Access Journal

Received June 16, 2020, accepted July 20, 2020, date of publication July 31, 2020, date of current version August 18, 2020.

Digital Object Identifier 10.1109/ACCESS.2020.3013304

Electromagnetic and Thermal Analysis of Cylindrical Aluminum Billet Heated by 1 MW HTS DC Induction Heater

XUFENG YAN, SHAOTAO DAI, AND TAO MA, (Member, IEEE)
School of Electrical Engineering, Beijing Jiaotong University, Beijing 100044, China

Corresponding author: Shaotao Dai (stdai@bjtu.edu.cn)

This work was supported in part by the National Key Research and Development Program under Grant 2017YFB0902302; in part by the National Key Research and Development Program under Grant 2017YFB0902302; in part by the National Natural Science Foundation of China under Grant 51477165; and in part by the Fundamental Research Funds for the Central Universities under Grant 2016RC039.

ABSTRACT In order to improve the efficiency of the conventional AC induction heater, an HTS DC induction heating technology has been proposed. A 1 MW HTS DC induction heater has been developed, and the efficiency of the HTS DC induction heater can be more than 80% due to the HTS DC magnet with no AC loss. The electromagnetic and thermal analysis of the HTS DC induction heater is necessary for further optimization of the 1 MW HTS DC induction heater. A 3D finite element simulation model for the coupling analysis of electromagnetic and thermal has been built based on the actual 1 MW HTS DC induction heater and optimized for accelerating the computing speed by using permanent magnet instead of the HTS magnet. The heating process of the cylindrical aluminum billet has also been simulated and compared with the experimental results. The results show that the simulation results can be in line with the experimental results. What is more, the optimized simulation model can be used to further optimize the device parameters for different workpiece temperature distributions, or design and evaluate the new HTS DC induction heater in the future.

INDEX TERMS Induction heating, high temperature superconductor (HTS), aluminum, direct current (DC), electromagnetic and thermal analysis.

I. INTRODUCTION

Alternative current (AC) induction heating technology is widely used to soften the aluminum billet before extrusion in aluminum extrusion plants. In order to avoid local melting or cracking during the extrusion of the aluminum billet, which will seriously affect the quality of the aluminum profile products, good temperature uniformity in cylindrical aluminum billet is required. Usually, the aluminum billet needs to be heated to 723.15 - 773.15 K, and the temperature deviation needs to be within ±2.5 percent [1]. However, the efficiency of converting input power into heating power is low, even the efficiency for the AC induction heaters rated at 1 MW can just be up to 60%, and the remaining energy is taken away by the cooling water flowing through the hollow copper coil [2], [3]. An HTS DC induction heating concept has been proposed to improve efficiency [2]. In the concept, the workpiece rotates in a static transverse magnetic field. According to Faraday's law and Lenz's law, the current will be induced in the workpiece to oppose the rotation of the workpiece. And the induced current in the workpiece will generate the Joule heat to heat the workpiece. The workpiece can be forced to rotate by a motor, and the magnetic field will be created by an HTS magnet excited by DC. Therefore, the HTS magnet has no AC loss, and the efficiency of the HTS DC induction heater is basically the same as that of the motor, which can be above 90% for the motors rated at 1 MW [4]. And the HTS magnet excited by DC is more reliable and safe than the one by AC, which makes the HTS DC induction heater one of the most promising superconducting devices for large-scale commercial applications.

The electromagnetic and thermal analysis for the HTS DC induction heating has been reported in many papers [5]–[7]. But the aluminum billets are smaller than the one with a diameter of 200 mm and a length of 1000 mm. So compared to the HTS DC induction heaters that can preheat larger aluminum

The associate editor coordinating the review of this manuscript and approving it for publication was Lei Chen.

billets, the simulation models have fewer finite element units, which will take less calculation time. The first commercial MW-class HTS DC induction heater for preheating large aluminum billets has been designed years ago and assembled in early 2019 [8]–[10]. And it has been designed to preheat the aluminum billets with diameters of 200 - 446 mm and lengths of 800 - 1760 mm. The 3D finite element simulation model built for the 1 MW HTS DC induction heater is more complicated, and the calculation quantity is huge, which will take a lot of time and resulting in low computational efficiency. Therefore the optimization of the 3D finite element simulation model for the electromagnetic and thermal analysis of the 1 MW HTS DC induction heater is very necessary for further optimization of the device parameters.

In this work, the 3D finite element simulation model for 1 MW HTS DC induction heater has been built and optimized by adding the additional iron core and replacing the HTS magnet with the permanent magnet (PM) to reduce the calculation quantity and accelerate the computing speed. The magnetic fields of the heating area generated by the two models with the HTS magnet and the PM respectively have been compared. And the power, torque, and temperature curves over time from simulations and experiments have also been compared. This optimized simulation model can be used for further designing and evaluating the 1 MW HTS DC induction heater, or designing the new larger HTS DC induction heater in the future.

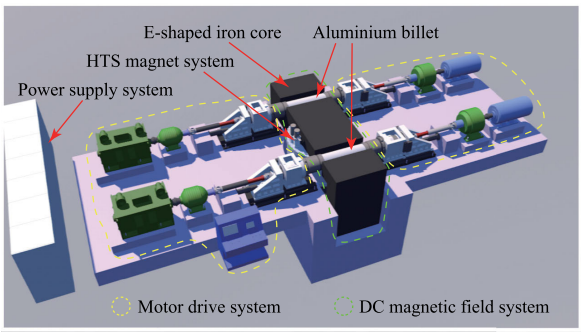

FIGURE 1. Structure diagram of the 1 MW HTS DC induction heating system, including the power supply system, the DC magnetic field system, and the motor drive system.

II. 1 MW HTS DC INDUCTION HEATER

Considering the potential on the energy and cost saving, a 1 MW HTS DC induction heater has been developed years ago and assembled in early 2019. Fig.1 shows the structure diagram of the 1 MW HTS DC induction heating system, which consists of three subsystems:

1) The power supply system provides the energy needed during the heating process for the whole system;
2) The DC magnetic field system generates the DC magnetic field in the two airgaps of E-shaped iron core by utilizing the HTS magnet excited by DC;
3) The motor drive system drives the aluminum billet to rotate in the DC magnetic field. And in order to solve the large torque appearing at a low rotation speed, the motor drive system adopts an auxiliary motor system except for the main motor system [11].

The iron core guides the magnetic field to the billets and shields other rotating metal components from both being exposed to the magnetic field and thereby being heated. Two aluminum billets, which can be heated simultaneously, are placed in the two separate air gaps.

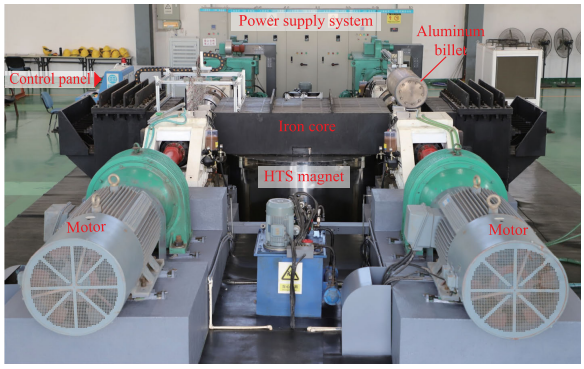

FIGURE 2. The picture of the 1 MW HTS DC induction heater.

The picture of the 1 MW HTS DC induction heater is shown in Fig.2. Based on the heater, several aluminum billets with different sizes have been tested. And the efficiency of the heater can reach up to 80%. The HTS magnet consists of three solenoid coils wound with 18 km YBCO superconducting tape from Shanghai Superconductor. Three solenoid coils array along the normal direction of the coils with a short distance between each one. The HTS magnet is cooled by two AL325 cryogenic refrigerators.

The inner and outer diameters of the YBCO magnet are Ø1960 mm and Ø2009 mm, respectively. The magnetic flux density at the center of the aluminum billet is 0.46 T at the operating current of 120 A. The specifications of the 1 MW HTS DC induction heater are given in Table 1.

TABLE 1. Specifications of the 1 MW HTS DC induction heater.

Items	Specifications
Metal billet type	Aluminum Billet (6061)
Average temperature	723.15 - 773.15 K
Temperature deviation	$\leq \pm 25$ K
Rotating speed	200 - 450 rpm
Billet size (Max.)	Ø446×1350 - 1700 mm
Rated power	500 kW×2
HTS (YBCO) tape	Shanghai Superconductor
Operating current	120 A
Magnetic field at the billet center	0.46 T
Inner\outer diameters of HTS magnet	Ø1960 mm\Ø2009 mm
Operating temperature	25 - 30 K
Room temperature	303 K

III. OPTIMIZATION OF 3D FINITE ELEMENT MODEL

A. SignifICANCE OF THE MODEL OPTIMIZATION

Several experiments have been done based on the 1 MW HTS DC induction heater. It has been found that the temperature distributions of the workpiece under different conditions, including the air gap structures, the excitation parameters,

and the motor speeds, are different, which is closely related to the material properties of the heated workpiece. The actual extrusion process has a great difference in the temperature distribution requirements of the workpiece, so it is impossible to obtain the adjustment parameters of the equipment through experiments. If an accurate simulation model can be established, on which rapid simulation analysis can be carried out based in advance, then the corresponding equipment regulation parameters can be obtained for different heating requirements, such as the parameters for adjusting the air gap magnetic field distribution by the iron core, adjusting excitation magnetomotive force by the superconducting coil and adjusting drag speed by the motor, and other parameters. It can be seen that the simulation can significantly reduce the number of experiments and experimental costs, but it should have the following characteristics:

1) The simulation model can truly reflect the experimental conditions, and only the 3D model can reflect the real state of the workpiece;
2) Due to the long time simulation of more than 10 minutes, the calculation quantity of the 3D model is huge, so the established model should meet the requirements of speedability while being accurate.

Therefore it is necessary to simplify and optimize the 3D finite element simulation model for decreasing the calculation quantity while being accurate.

B. GEOMETRY

Fig.3 shows the 3D finite element simulation model. The complete simulation model with the HTS magnet is given as shown in Fig.3(a), and the air domain is not displayed. The simulation model is based on the practical 1 MW HTS DC induction heater to establish. Based on the geometry symmetry, a 1/4 model showed in Fig.3(b) is adopted to simplify the simulation model. The practical HTS magnet has three HTS coils, which are combined into one in the model, and thus can simplify the model. The combination hardly affects the magnetic field distribution in the heating area and can reduce the calculation quantity of the simulation model. The additional iron core showed in Fig.3 does not exist in the practical heater. Here it is arranged to improve the mesh of the model and thereby decrease the number of the mesh elements because the center cylindrical iron core is tangent to sides of the iron core, which can be seen in Fig.3.

It can be seen from Fig.4 that the number of the meshes of the model without the additional iron core is larger than the model with the additional iron core, and the number of the fine mesh of the former is fewer than the latter. The decrease of the fine meshes and the fewer meshes can effectively reduce the calculation quantity and shorten the computing time. The simulation model has two kinds of computing domains in the simulation model, including the domain of the ampere's law and the domain of the conservation of magnetic flux. And the domain of the ampere'law includes the HTS magnet domain and the aluminum domain. The boundaries

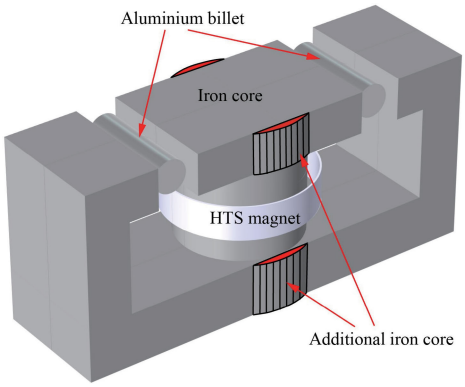

(a) Simulation model with the HTS magnet and the additional iron core.

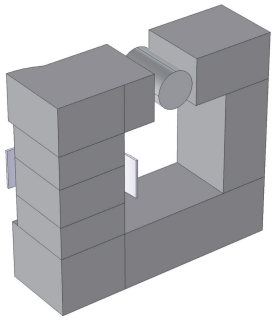

(b) 1/4 simulation model with the HTS magnet and the additional iron core.

FIGURE 3. 3D finite element simulation model.

between the two kinds of domains are mixed boundaries, which will complicate the calculation. And the HTS magnet has a large length ratio, which will result in the finer meshes and thereby increase the calculation quantity and the computing time.

To further simplify the simulation model and shorten the computation time, an optimization method is proposed, that is, the HTS magnet is replaced by a PM, which has been shown in Fig.5(a). And a quarter model is adopted as well, which can be seen in Fig.5(b). Thus the domain of the ampere'law has only aluminum domain. And the meshes of the model are also optimized by add the additional iron core. The height and the radius of the PM are as equal as the height of the HTS magnet and the radius of the central iron core, respectively. And the magnetization M of the PM is set as a multiple k of the ampere-turns of the HTS magnet. The k value can be determined by comparing the magnetic field in the heating area with that generated by the model with the HTS magnet using the method of trials and errors. And the value of k is unique for a given operating current. In this method, the HTS magnet is far away from the heating area in the magnetic circuit. If the HTS magnet is near the heating area in the magnetic circuit, the method proposed will not be applicable because the magnetic flux leakage of the HTS magnet will have a great influence on the magnetic field distribution in the heating area.

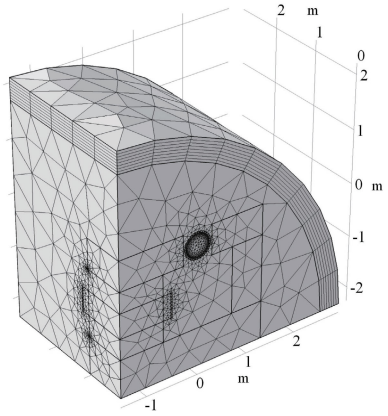

(a) Mesh of the simulation model without the additional iron core.

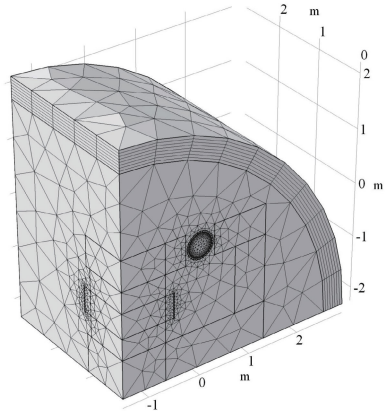

(b) Mesh of the simulation model with the additional iron core.

FIGURE 4. Mesh of the simulation models.

TABLE 2. Comparison of the number of finite elements for the two models.

Items	Number of elements
1/4 Model with HTS magnet, no additional iron	91724
1/4 Model with HTS magnet, additional iron	90519
1/4 Model with PM, additional iron	38900

The mesh of the 1/4 model with the PM is shown in Fig.6. It can be seen that the number of mesh elements of the model with the PM is less than the model with the HTS magnet. The number of mesh elements for the two models under the same meshing settings is shown in Table 2. It can be seen that the model with the PM has 57% fewer mesh elements than the model with the HTS magnet, which is related to the setting of mesh. Fewer finite elements will effectively reduce the calculation quantity and speed up the calculation.

C. NUMERICAL METHOD

The heating process of the aluminum billet involves two physical analysis processes: the electromagnetic analysis process and the thermal analysis process. And the two physical processes are closely related. The temperature change of the aluminum billet is driven by the resistance heating of the induced current in the aluminum billet, the current

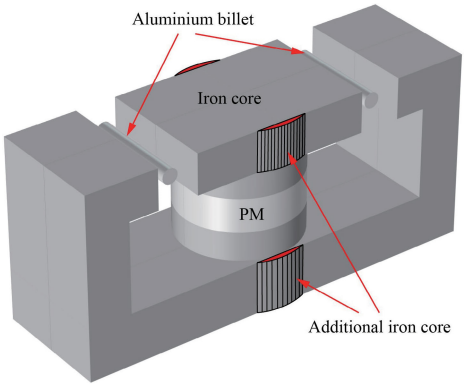

(a) Simulation model with the PM and the additional iron core.

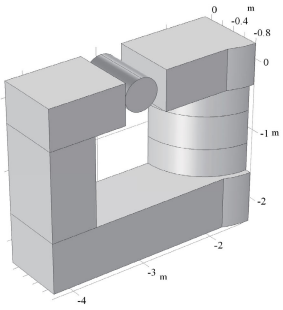

(b) 1/4 simulation model with the PM and the additional iron core.

FIGURE 5. The simulation model using the PM instead of the HTS magnet.

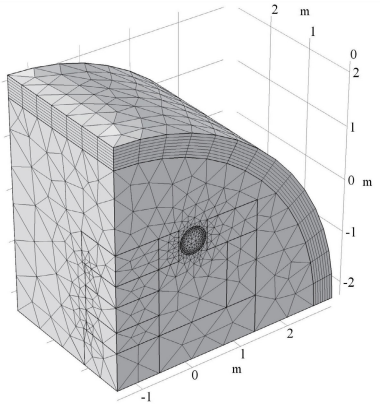

FIGURE 6. Mesh of the 1/4 simulation model with the PM.

distribution depends on the electrical conductivity, and the electrical conductivity depends on the temperature. In other words, the heating process is a two-way coupling process of the two physical processes. In order to analyze the heating process of the aluminum billet, the heating process will be discretized into a series of fine time steps. In each time interval, the physical parameters of the aluminum billet can be assumed to be constant because the temperature change can be negligible, which hardly affects the induced current density distribution in the aluminum billet [1], [11]. Therefore, the electromagnetic analysis process is a steady-state, and the physical parameters of the aluminum billet keep

constant in each time interval. The induction power density distribution can be got in the electromagnetic analysis, which will be used as the heat source in the thermal analysis. And the new temperature distribution will be obtained in the thermal analysis, which will be used as the initial value in the next time interval, and the physical parameters of the aluminum billet will also be updated [7]. Fig.7 shows the calculation process of heating the aluminum billet.

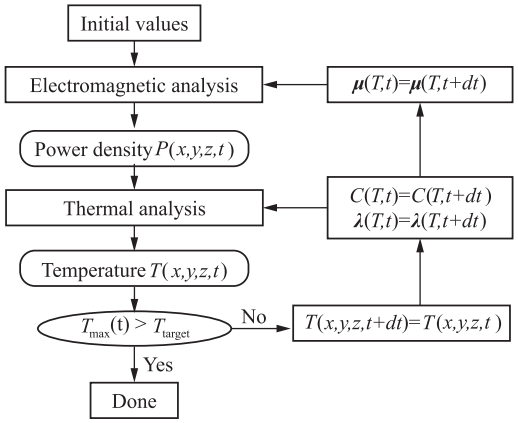

FIGURE 7. Calculation process of heating the aluminum billet.

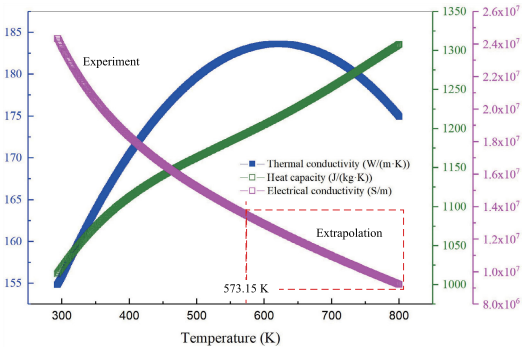

FIGURE 8. Temperature dependence of the aluminum alloy 6061's electrical and thermal parameters.

The temperature dependence of the aluminum billet's electrical and thermal parameters are shown in Fig.8. The electrical conductivity is from [6], but the temperature range is only from 293.15 K to 573.15 K, and the electrical conductivity after 573.15 K is derived from extrapolation. The thermal conductivity and the heat capacity is from the software materials. The density of the aluminum billet is 2700 kg/m^3, which is constant because of negligible size changes of the aluminum billet caused by the thermal effect. The relative permeability is a constant of 1, which is hardly affected by the varying temperature. The convective heat transfer has also been considered, which is related to the rotation speed of the aluminum. The convection heat transfer coefficient α can be expressed by the relationship [5]:

$$\alpha \approx 20 \times \upsilon^{0.54} \tag{1}$$

with: α - convection heat transfer coefficient (W/m^{2}K) and υ - peripheral speed (m/s). The thermal radiation is neglected due to the weak influence during the heating process [7].

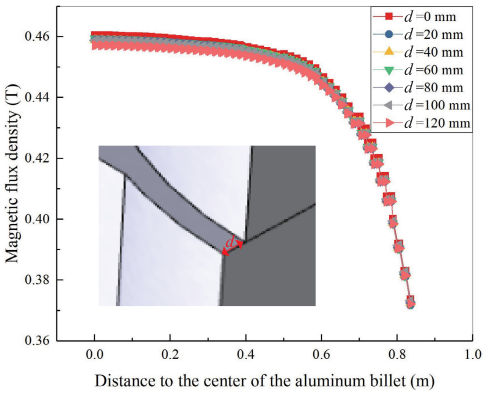

(a) Magnetic flux density along the axis of the aluminum billet in the model with the HTS magnet.

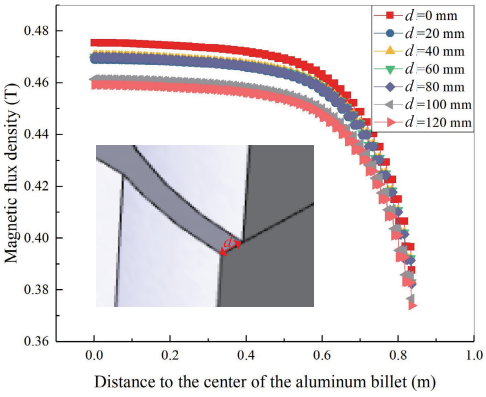

(b) Magnetic flux density along the axis of the aluminum billet in the model with the PM.

FIGURE 9. The magnetic field along the axis of the aluminum billet.

IV. RESULTS AND DISCUSSION

A. COMPARISON OF THE MAGNETIC FIELD

The magnetic field along the axis of the aluminum billet for the varying d ranging from 0 to 120 mm is shown in Fig.9. The d represents the size of the additional iron core, and the larger d is, the less the fine mesh is. It can be seen that the additional iron core has a weak influence on the magnetic flux density in the heating area. With the increase of d, the magnetic flux density in the heating area decreases little. When d is 120 mm, the magnetic flux density decreases by 0.6% compared with that when d is 0 mm in the model with HTS magnet, which can be seen in Fig.9(a). And when d is 100 mm, the magnetic flux density decreases by 1.6% compared with that when d is 0 mm in the model with PM, which can be seen in Fig.9(b). Therefore, the magnetic flux density deviation caused by the additional iron core can be negligible. This because the magnetomotive forces are the same, and the iron core is mainly used to guide the magnetic force lines to the heating area. Local changes of the iron core do not affect the magnetic flux density distribution in the heating area. And d is 100 mm in the following simulation analysis unless there is a specific explanation.

The value of k in the model with the PM can be determined by comparing the magnetic fields along the axis of

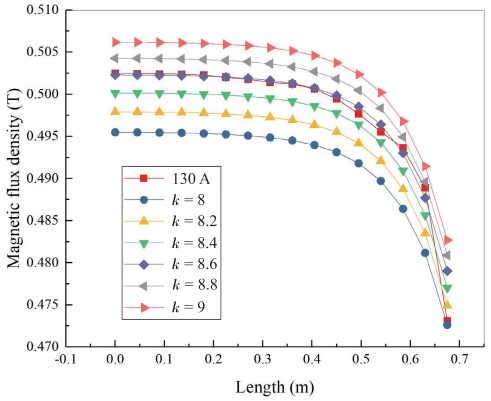

FIGURE 10. Determination of the k value for the operating current of 130 A by comparing the magnetic field along the axis of the aluminum billet using the method of trials and errors.

the aluminum billet with that generated by the model with the HTS magnet using the method of trials and errors. Fig.10 shows the determination of k value for the operation current of 130 A. And the corresponding k for 130 A is 8.6. The deviation of the magnetic fields from the two models at the end of the axis of the aluminum billet is 1.24%. The k value for 130 A was finally determined to be 8.61 after further adjustment, and the deviation is 0.98%.

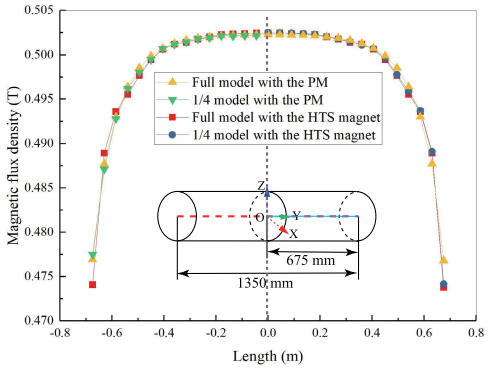

FIGURE 11. Magnetic flux densities along the axis of the aluminum billet generated by the full model and 1/4 model.

The magnetic flux densities along the axis of the aluminum billet generated by the full model and 1/4 model with the HTS magnet and the PM respectively are shown in Fig.11. The operating current is 130 A, and the corresponding k is 8.61. It can be seen that the magnetic flux densities generated by the full model and 1/4 model match well, indicating that the 1/4 model based on symmetry is right and feasible.

The magnetic flux density distributions of the 1/2 aluminum billet with a diameter of 446 mm and a length of 1350 mm are shown in Fig.12, and the symmetrical plane is the zx plane. The Fig.12(a) shows the magnetic flux density distribution of the 1/2 aluminum billet in the 1/4 model with the HTS magnet when the operating current is 130 A. And Fig.12(b) shows the magnetic flux density distribution of the 1/2 aluminum billet in the 1/4 model with the PM when the corresponding k is 8.61. It can be seen that the magnetic flux density distributions of the aluminum billet in two models

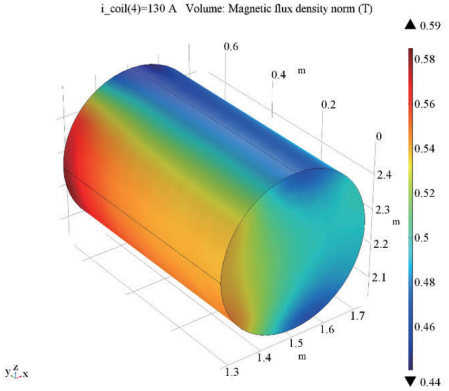

(a) Magnetic flux density distribution of the aluminum billet in the 1/4 model with the HTS magnet, and the operating current is 130 A.

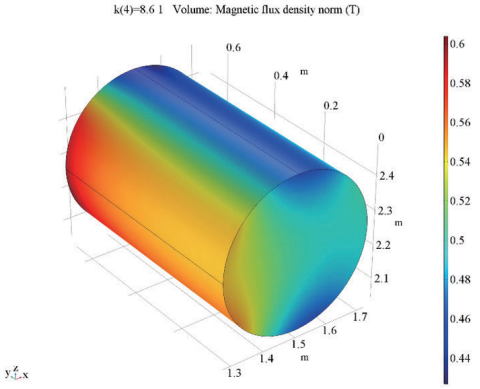

(b) Magnetic flux density distribution of the aluminum billet in the 1/4 model with the PM, and the corresponding k is 8.61.

FIGURE 12. The magnetic flux density distribution of the aluminum billet with a diameter of 446 mm and a length of 1350 mm.

are very similar, and the maximum magnetic flux density of the latter is 1.7% larger than the former. And the deviation between the magnetic flux density distributions in the heating area of the two models can be further reduced by further adjusting the value of k.

In order to further illustrate that the model with the HTS magnet can be replaced by the model with the PM, the magnetic flux densities generated by the two models on the axis and the surface of the aluminum billet has been compared. The diameter and length of the aluminum billet are 446 mm and 1350 mm, respectively. The current of the HTS magnet is 120 A, and the corresponding k is 8.875. The magnetic flux density along the axis of the aluminum billet in the two models are plotted as a function of distance to the center of the aluminum billet in Fig.13. It can be seen that the curves of the magnetic flux density generated by the two models along the axis of the aluminum billet almost overlap.

The magnetic flux densities along the length on the surface of the aluminum billet at eight different positions are also compared, which can be seen in Fig.14. The curves of the magnetic flux density generated by the two models also basically overlap, and the maximum deviation of the

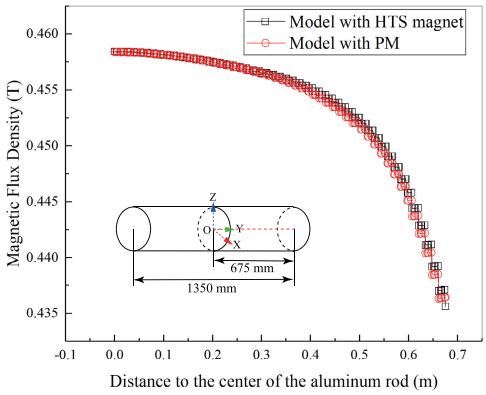

FIGURE 13. Magnetic flux density along the axis of the aluminum billet.

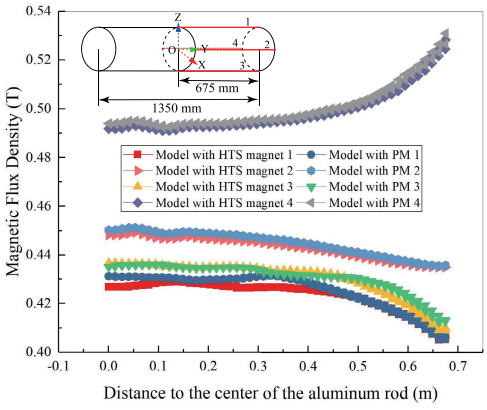

(a) Magnetic field along the aluminum billet surface at four different positions.

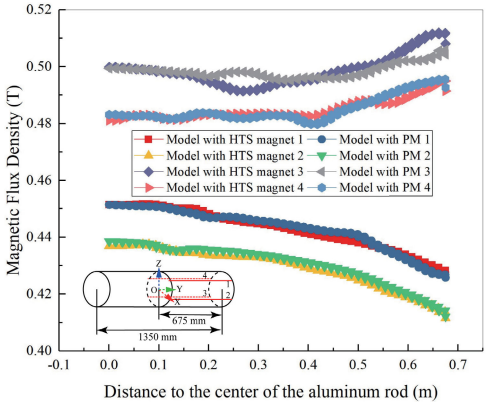

(b) Magnetic field along the aluminum billet surface at other four different positions.

FIGURE 14. Comparison of the magnetic flux density in the heating area of the aluminum billet between the two models.

magnetic flux density is 1.7%, which can be acceptable. The non-smooth curves are mainly caused by the meshing of the model. According to Fig.13 and 14, it can be preliminary decided that the method of using the PM instead of the HTS magnet in the model is reasonable and feasible.

B. COMPARISON OF THE COMPUTING TIME

In order to verify that replacing the HTS magnet with a PM does reduce the computing time, the computing time of heating the aluminum billet for 5 s is compared. Both the two models have the additional iron core, and the rotation speed of the aluminum billet is a constant of 400 rpm. The configuration of the used computer is Intel(R) Core(TM) i7-8650U CPU @ 1.90 GHz 2.11 GHz and a 16.0 GB RAM. The computing time and the basic specifications for the 1/4 model with the HTS magnet and the PM respectively are given in Table 3. It can be seen that replacing the HTS magnet with a PM can decrease the number of mesh elements of the model and reduce the computing time effectively.

TABLE 3. Comparison of the computing time and the basic specifications.

Items	Model with HTS magnet	Model with PM
Number of elements	139059	123160
Additional iron	Yes	Yes
Size of the billet	Ø446×1350 mm	Ø446×1350 mm
Current	130 A	-
k value	-	8.861
Rotation speed	400 rpm	400 rpm
Heating time	5 s	5 s
Computing time	19 h	13 h

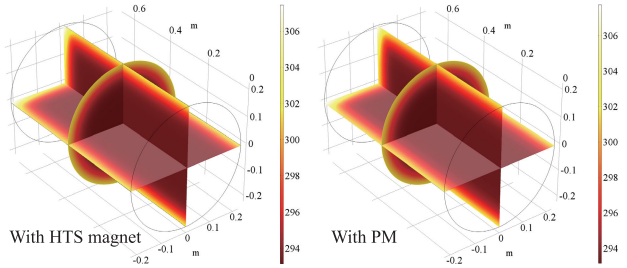

FIGURE 15. Temperature distributions of the aluminum billets from the two models.

Fig.15 shows the temperature distributions of the aluminum billet from the two models at the heating time of 5 s, from which it can be seen that the temperature distributions match well, indicating that using the PM instead of the HTS magnet in the model is reasonable and feasible.

C. VALIDATION OF THE OPTIMIZED MODEL

The aluminum billet heated by the 1 MW HTS DC induction heater has a diameter of 446 mm and a length of 1500 mm. And the rotation speed of the aluminum billet at the operating current of 120 A increases from zero to a peak of 400 rpm within 127 s and keeps constan after 127 s, which is shown in Fig.16. The start time of the motor depends on the load, including the operating current of the HTS magnet and the different aluminum billets. The curve of the rotation speed over time is adopted in the simulation model.

Fig.17 shows the simulation and experimental magnetic field results at the center of the aluminum billet for different operating currents ranging from 40 A to 120 A. The magnetic field results obtained by the 1/4 and full models with the HTS magnet and with the PM respectively are consistent with the experimental results, which indicates that replacing the full model with the 1/4 model is feasible. The magnetic flux density at the center of the aluminum billet is 0.46 T when the operating current is 120 A and the corresponding k is 8.875.

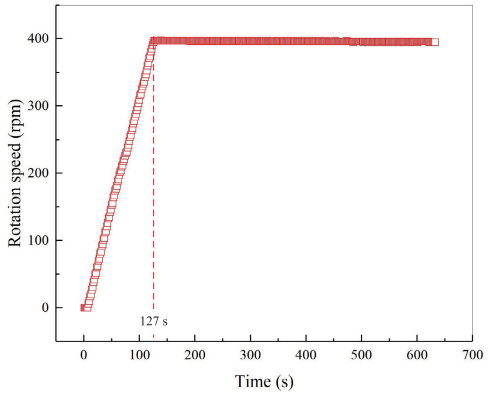

FIGURE 16. Rotation speed of the aluminum billet when the operating current is 120 A.

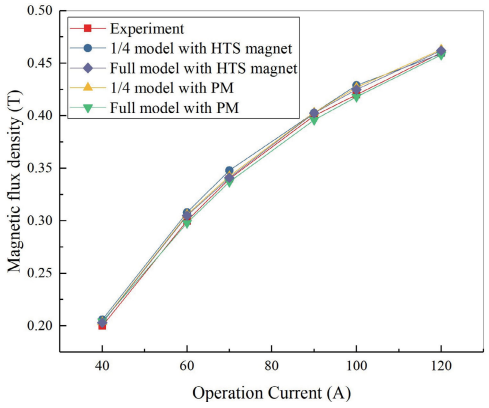

FIGURE 17. Magnetic field at the center of the aluminum billet for different operating currents.

Fig.18 shows the current density, power density, and temperature distributions of the 1/2 aluminum billet at the time of 525 s, and the symmetrical plane is *zx* plane. The current density and power density distributions are similar. It can be seen from Fig.18(a) and (b) that the current density and the power density concentrate on the surface layer of the aluminum billet because of the skin effect. The arrows in Fig.18(a) represents the direction of the induced current. The temperature distribution is shown in Fig.18(c). It can be seen that the temperatures at the ends of the aluminum billet is larger than the middle domain, which is in line with the experimental result in Fig.18(d). The temperature distribution on the aluminum billet surface is measured by a thermal imager during the heating process. The simulation temperatures at the surface center and the end of the aluminum billet are 637 K and 775 K respectively, and the corresponding experimental temperatures are 648 K and 775 K respectively. The experimental temperature difference on the billet surface is smaller than the simulation result because the simulation model does not consider the metal parts fixing the billet to rotate.

The simulation and experimental results of the heating power and the torque at the operating current of 120 A during the heating process are shown in Fig.19. The total input power of the main and auxiliary motors and the heating power

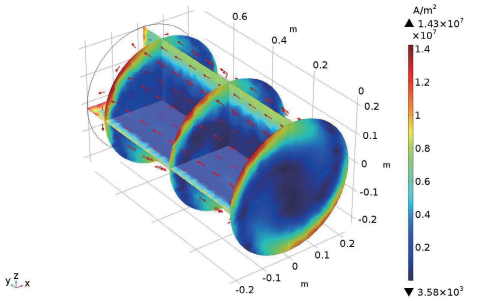

(a) Current density distribution.

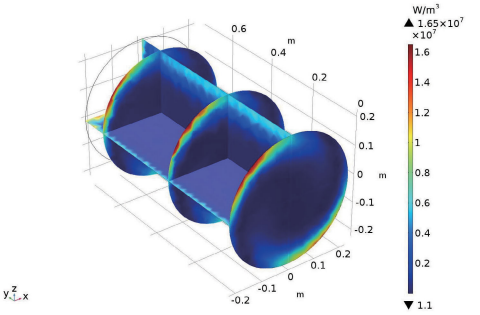

(b) Power density distribution.

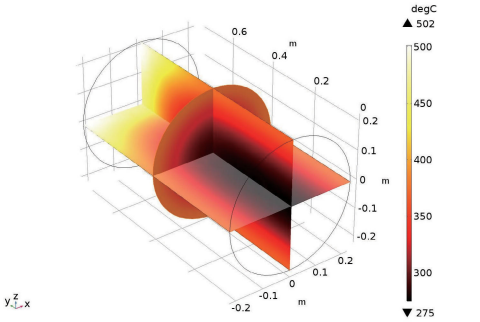

(c) Temperature distribution.

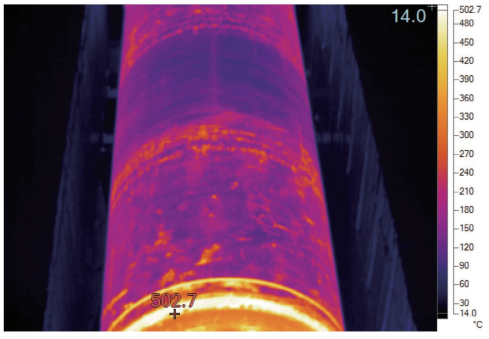

(d) Experimental temperature.

FIGURE 18. The current, power, and temperature distributions of the 1/2 aluminum billet at the time of 525 s.

obtained by simulation are plotted as a function of the time in Fig.19(a). Considering the efficiency of the motor, the heating power entered into the aluminum billet is 90% of the total input power, which matches well with the simulation heating power before 400 s. And the simulation heating power after 400 s does not increase linearly because the

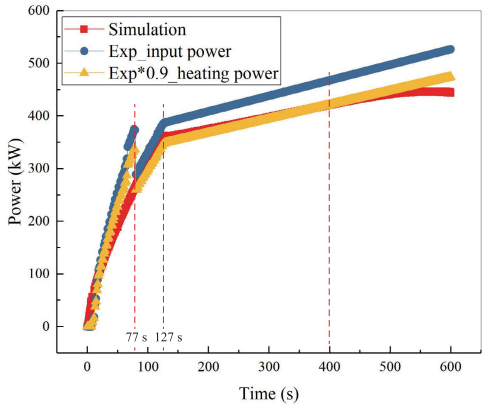

(a) Simulation and experimental results of the power.

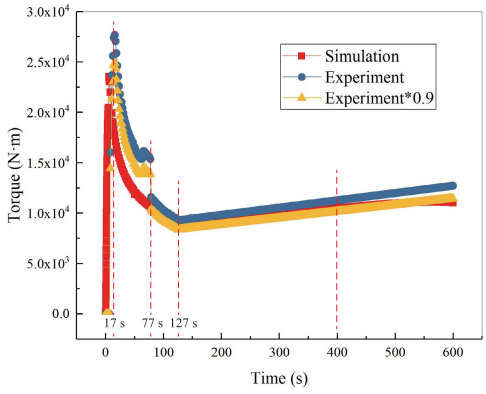

(b) Simulation and experimental results of the torque.

FIGURE 19. Simulation and experimental results of the torque and power at the operating current of 120 A.

thermal conductivity starts to fall with the temperature after 573.15 K, and the electrical conductivity of the aluminum billet after 573.5 K is derived from extrapolation. It can also be seen that the input power increases fast before 127 s due to the linear increase in rotation speed, and increases slowly after 127 s because of the temperature dependence of the electrical conductivity. The rotation speed of the aluminum billet reaches up to the maximum 400 rpm at 127 s and keep constant after 127 s. It can be seen that the varying trend of the power agrees with the rotation speed of the aluminum billet. But the experimental power curve has a sudden drop at 77 s because of the auxiliary motor no longer works after 77 s. The experimental and simulation torques are shown in Figure 19(b). It can be seen that the torque has a maximum value at 17 s, at which the rotation speed is 38 rpm. This is consistent with the conclusions in [12]. And the relationship between the heating power and the torque can be expressed by the following equation:

$$T = 9950 * P/n \tag{2}$$

with: T - torque (N·m), P - heating power (W), and n - rotation speed (rpm). Therefore, the reason for the torque curves varying after 127 s is the same as the power.

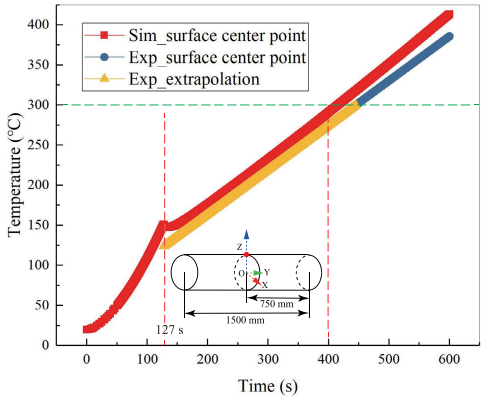

FIGURE 20. Simulation and experimental temperature results of the billet at the operating current of 120 A.

Fig.20 shows the simulation and experimental temperature results at the surface center point of the aluminum billet during the heating process. It can be seen that the simulation and experimental temperatures at the surface center point (red point) of the aluminum billet match well before 400 s, and the slope of the simulation temperature curve gradually increases after 400 s, which is consistent with the power and torque, and also because of the temperature dependence of physical parameters of the aluminum billet, especially the thermal conductivity and electrical conductivity. The thermal conductivity begins to fall with the temperature after 573.15 K. The electrical conductivity of the aluminum billet, which is a function of the temperature, is obtained in [6]. But the temperature ranges only from 293.15 K to 573.15 K. The electrical conductivity is derived from extrapolation when the temperature is larger than 573.15 K. And the simulation temperature is 6.7% larger than the experimental temperature at 600 s.

The influences of replacing the HTS magnet with the PM on the operation loss, volume, and weight of the heater are not taken into account because the PM is just an equivalent setting for simplifying the simulation model and does not apply in the actual. According to the comparisons between the simulation and experimental results, the optimized model is feasible, which can be used to further evaluate and optimize the 1 MW HTS DC induction heater.

V. CONCLUSION

A 3D finite element simulation model for 1 MW HTS DC induction heater has been built for the electromagnetic and thermal analysis of the heater. In order to reduce the calculation quantity and accelerate the computing speed, the 3D simulation model has been optimized by adjusting the geometry of the model properly and replacing the HTS magnet with a PM. The simulation results show that the magnetic flux density distributions generated by the two models in the heating area of the aluminum billet are the same.

The HTS magnet is used to provide the magnetomotive force required for the background field in the heating area. The simulation and experimental results show that the change

of the magnetic field induced by the rotation of the workpiece has little influence on the magnetic field in the iron core and the magnetomotive forces of the excitation system. The key to the method is that the constant magnetomotive force is set in the iron core, and the magnetomotive force has little dependence on how the magnetomotive force is generated. Although the actual system can not use the PM to produce such a large magnetomotive force, it does not affect the equivalent setting in the simulation model. The advantage of this equivalent setting is that the model can avoid too small mesh resulted from the thin HTS magnet increasing dramatically the calculation quantity of the simulation model. The mesh elements of the model with the PM reduce by 57% than the model with the HTS magnet, which is related to the setting of mesh.

The validation of the simulation model with the PM has also been verified by the experimental results. This method proposed is applicable for the case that the HTS magnet is far away from the heating area in the magnetic circuit. And the optimized simulation model and the optimization method can be used for further optimizing and evaluating the device parameters of the 1 MW HTS DC induction heater under different workpiece temperature distributions, or designing the new larger HTS DC induction heater in the future.

REFERENCES

[1] M. Fabbri, A. Morandi, and P. Luigi Ribani, "DC induction heating of aluminum billets using superconducting magnets," *Compel Int. J. Comput. Math. Electr. Electron. Eng.*, vol. 27, no. 2, pp. 480–490, Mar. 2008.

[2] N. Magnusson, R. Bersås, and M. Runde, "Induction heating of aluminum billets using HTS DC coils," *Inst. Phys. Conf. Ser.*, vol. 181, pp. 1104–1109, Sep. 2004.

[3] M. Fabbri, A. Morandi, and P. Luigi Ribani, "Operational constraints on the DC induction heating of aluminum billets," *Compel Int. J. Comput. Math. Electr. Electron. Eng.*, vol. 30, no. 5, pp. 1589–1597, Sep. 2011.

[4] A. Morandi, M. Fabbri, and P. L. Ribani, "Design of a superconducting saddle magnet for DC induction heating of aluminum billets," *IEEE Trans. Appl. Supercond.*, vol. 18, no. 2, pp. 816–819, Jun. 2008.

[5] R. Araneo, F. Dughiero, M. Fabbri, M. Forzan, A. Geri, A. Morandi, S. Lupi, P. L. Ribani, and G. Veca, "Electromagnetic and thermal analysis of the induction heating of aluminum billets rotating in DC magnetic field," *Compel Int. J. Comput. Math. Electr. Electron. Eng.*, vol. 27, no. 2, pp. 467–479, Mar. 2008.

[6] Y. Wang, J. Yang, Z. Y. Li, Z. Jin, and Z. Hong, "Study on a numerical method for calculating the heating process of HTS DC induction heater," *IEEE Trans. Appl. Supercond.*, vol. 24, no. 3, pp. 1–5, Jun. 2014.

[7] Y. Wang, H. Gao, Z. Li, Y. Ping, Z. Jin, and Z. Hong, "Study of the temperature uniformity of aluminium billets heated by superconducting DC induction heaters," *Compel Int. J. for Comput. Math. Electr. Electron. Eng.*, vol. 34, no. 1, pp. 357–370, Jan. 2015.

[8] Y. Wang, Y. Ping, K. Li, H. Song, J. Yang, C. Ma, Z. Jin, and Z. Hong, "Analysis and comparison between no-insulation and metallic insulation REBCO magnet for the engineering design of a 1-MW DC induction heater," *IEEE Trans. Appl. Supercond.*, vol. 27, no. 4, pp. 1–5, Jun. 2017.

[9] D. Zhang, G. Zhang, L. Lin, L. Xiao, N. Song, L. Jing, X. Wang, S. Liang, Q. Li, Y. Teng, and J. Zhang, "Research on the conduction-cooled YBCO magnet for an MW class induction heating system," *IEEE Trans. Appl. Supercond.*, vol. 28, no. 3, pp. 1–5, Apr. 2018.

[10] P. Yang, Y. Wang, D. Qiu, T. Chang, H. Ma, J. Zhu, Z. Jin, and Z. Hong, "Design and fabrication of a 1-MW high-temperature superconductor DC induction heater," *IEEE Trans. Appl. Supercond.*, vol. 28, no. 4, pp. 1–5, Jun. 2018.

[11] M. Fabbri, A. Morandi, and F. Negrini, "Temperature distribution in aluminum billets heated by rotation in static magnetic field produced by superconducting magnets," *Compel Int. J. Comput. Math. Electr. Electron. Eng.*, vol. 24, no. 1, pp. 281–290, Mar. 2005.

[12] P. Yang, S. Dai, T. Ma, J. Huang, G. Jiang, Y. Wang, Z. Hong, and Z. Jin, "Analysis of peak electromagnetic torque characteristics for superconducting DC induction heaters," *IEEE Access*, vol. 8, pp. 14777–14788, 2020.

XUFENG YAN was born in Shanxi, China, in 1989. He received the B.S. degree in electrical engineering and automation from the Institute of Disaster Prevention, Hebei, China, in 2013, and the M.S. degree in electrical engineering from Beijing Jiaotong University, Beijing, China, in 2017, where he is currently pursuing the Ph.D. degree.

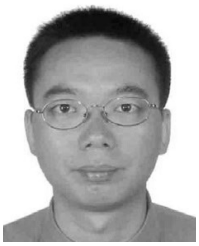

SHAOTAO DAI was born in Jiangxi, China, in 1972. He received the B.S. and M.E. degrees from Central South University, Changsha, China, in 1994 and 1997, respectively, and the Ph.D. degree from the Graduate School, Chinese Academy of Sciences, in 2010. He was a Professor with Beijing Jiaotong University, Beijing, China. He was a member of the Superconducting Applied Technology Professional Committee, China Electrotechnical Society. He is leading the research team in the area applied the application of HTS, including cables, fault current limiters, energy storage, machines, transformers, and power transmission lines.

TAO MA (Member, IEEE) was born in Hubei, China, in 1984. He received the B.S. degree in automation specialty and the Ph.D. degree in control science and engineering from the Beijing Institute of Technology University, Beijing, China, in 2006 and 2011, respectively. He has been an Associate Professor with Beijing Jiaotong University, Beijing, since 2016.